chemistry

MDPI

Article

From Frustrated Packing to Tecton-Driven Porous Molecular Solids

Chamara A. Gunawardana [1], Abhijeet S. Sinha [1], Eric W. Reinheimer [2] and Christer B. Aakeröy [1,*]

[1] Department of Chemistry, Kansas State University, Manhattan, KS 66506, USA; chamara@ksu.edu (C.A.G.); sinha@ksu.edu (A.S.S.)

[2] Rigaku Americas Corporation, 9009 New Trails Drive, The Woodlands, TX 77381, USA; eric.reinheimer@rigaku.com

* Correspondence: aakeroy@ksu.edu; Tel.: +1-785-532-6096

Received: 24 February 2020; Accepted: 10 March 2020; Published: 13 March 2020

Abstract: Structurally divergent molecules containing bulky substituents tend to produce porous materials via frustrated packing. Two rigid tetrahedral cores, tetraphenylmethane and 1,3,5,7-tetraphenyladamantane, grafted peripherally with four (trimethylsilyl)ethynyl moieties, were found to have only isolated voids in their crystal structures. Hence, they were modified into tecton-like entities, tetrakis(4-(iodoethynyl)phenyl)methane [**I_4TEPM**] and 1,3,5,7-tetrakis(4-(iodoethynyl)phenyl)adamantane [**I_4TEPA**], in order to deliberately use the motif-forming characteristics of iodoethynyl units to enhance crystal porosity. **I_4TEPM** not only holds increased free volume compared to its precursor, but also forms one-dimensional channels. Furthermore, it readily co-crystallizes with Lewis basic solvents to afford two-component porous crystals.

Keywords: crystal engineering; porous material; molecular recognition; halogen bond; co-crystal; molecular tecton; binary solid; network structure; σ-hole; molecular electrostatic potential

1. Introduction

According to Kitaigorodskii's principle of close packing [1–5], molecules in crystals tend to dovetail and pack as efficiently as possible in order to maximize attractive dispersion forces and to minimize free energy. In other words, void space in crystals is always unfavorable. Thus, the construction of porous materials from discrete organic molecules (i.e., molecular porous materials (MPMs)) demands some special tactics [6–11]. For example, the packing of molecules specifically designed to bear sufficiently large and dimensionally fixed inner cavities or clefts (e.g., molecular cages and bowl-shaped compounds) can lead to porous structures [12–14].

Another viable synthetic strategy towards MPMs is to employ molecules with bulky, divergent and/or awkward shapes so that they no longer have the ability to pack tightly. Molecules such as 4-*p*-Hydroxyphenyl-2,2,4-trimethylchroman (Dianin's compound) [15,16], tris(*o*-phenylenedioxy) cyclotriphosphazene (TPP) [17–19] and 3,3′,4,4′-tetrakis(trimethylsilylethynyl)biphenyl (TTEB) [20] are well-known for producing MPMs merely as a consequence of frustrated packing, even though they do not have pre-fabricated molecular free volumes.

We have now expanded this idea to a family of tetrahedral molecules substituted at the four vertices with bulky groups. Here, we report the synthesis and structural investigation of tetrakis(4-((trimethylsilyl)ethynyl)phenyl)methane (**TMS_4TEPM**) and 1,3,5,7-tetrakis (4-((trimethylsilyl)ethynyl)phenyl)adamantane (**TMS_4TEPA**) (Scheme 1). By affixing large trimethylsilylethynyl (TMS-acetylenyl) moieties to the parent tetraphenylmethane (TPM) and

1,3,5,7-tetraphenyladamantane (TPA) core units, our aim was to disturb close-packing and to realize more open crystalline solids.

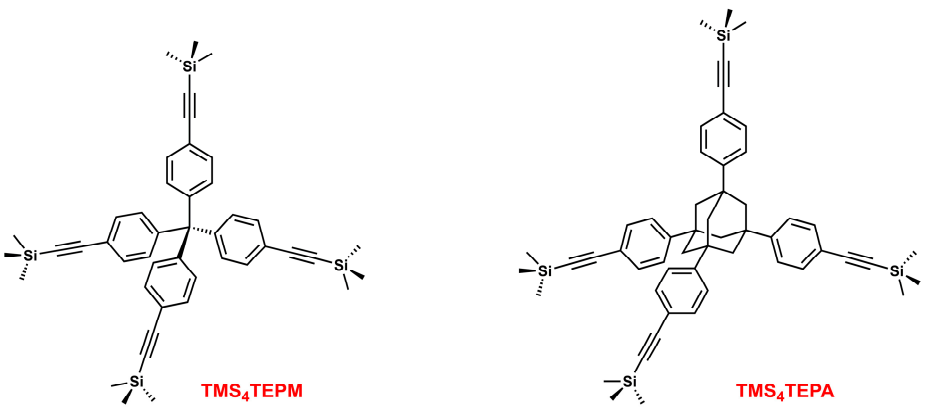

Scheme 1. Structural formulas of tetrakis(4-((trimethylsilyl)ethynyl)phenyl)methane (**TMS$_4$TEPM**) and 1,3,5,7-tetrakis(4-((trimethylsilyl)ethynyl)phenyl)adamantane (**TMS$_4$TEPA**).

Even though molecular shape is of primary importance in crystal packing, it is not the only structure-directing factor. The presence of functional units that can partake in directional and energetically significant non-covalent interactions has a major influence on molecular arrangement. With tectons (i.e., molecules featuring multiple peripheral binding sites) [21–24], the structure is built up so as to saturate the maximum amount of interactions, which is usually accompanied by compromises regarding dense-packing. Their association induces the assembly of networks where each molecule is positioned, through directional molecular recognition events, in a definite way with respect to its neighbors. Moreover, unlike van der Waals contacts, intermolecular point contacts consume only a limited amount of molecular surface, thereby leaving more usable surface. In this context, a great body of work has been done with hydrogen-bonding tectons to build so-called hydrogen-bonded organic frameworks (HOFs) [25–28]. Some notable examples include triptycenetrisbenzimidazolone (TTBI) [29], triaminotriazine-functionalized spirobifluorene [30,31] and polyfluorinated triphenylbenzene equipped with pyrazole [32].

Molecular tectonics based on halogen bonding (XB) is still in its infancy [33,34]. We therefore decided to modify the TPM and TPA scaffolds and transform them into new tecton-like entities, tetrakis(4-(iodoethynyl)phenyl)methane (**I$_4$TEPM**) and 1,3,5,7-tetrakis(4-(iodoethynyl)phenyl)adamantane (**I$_4$TEPM**) (Scheme 2). When iodine is directly bonded to an *sp*-hybridized carbon, it is strongly polarized, resulting in a more pronounced electron-deficient region (i.e., σ-hole) at the tip along the C–I bond axis [35–38]. The iodoethynyl functionality is, therefore, a perfect candidate for σ-hole/XB interactions. Alhough largely overlooked in molecular tectonics and crystal engineering, it can direct the assembly of network structures through C≡C–I···(C≡C) interactions (wherein the ethynyl π system acts as the XB acceptor) [39–41]. These T-shaped contacts frequently lead to *zigzag* chain motifs and are topologically parallel to those formed by C≡C–H···(C≡C) and C≡C–Br···(C≡C) contacts [37,42–52], but preferably serve as a stronger counterpart. Additional features that make the iodoethynyl unit well-suited for devising molecular building blocks include its structural rigidity, steric openness and core expanding ability.

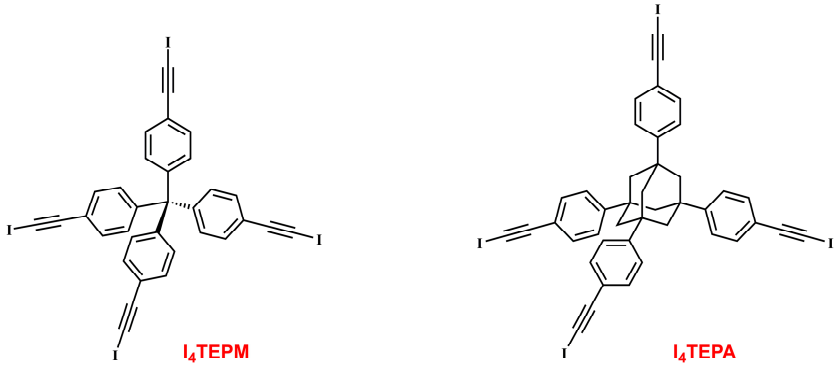

Scheme 2. Structural formulas of tetrakis(4-(iodoethynyl)phenyl)methane (**I$_4$TEPM**) and 1,3,5,7-tetrakis(4-(iodoethynyl)phenyl)adamantane (**I$_4$TEPM**).

2. Results and Discussion

The four molecules of interest were obtained according to the synthetic pathways shown in Schemes 3 and 4. Starting with commercially available tetraphenylmethane, **TMS$_4$TEPM** was prepared in two steps (tetra-*para*-bromination followed by coupling with trimethylsilylacetylene) with an overall yield of 78%. The synthesis of **TMS$_4$TEPA** required three steps (Friedel-Crafts reaction of 1-bromoadamantane and benzene, tetra-*para*-iodination followed by coupling with trimethylsilylacetylene), and the yield over these three steps was 50% (with respect to 1-bromoadamantane).

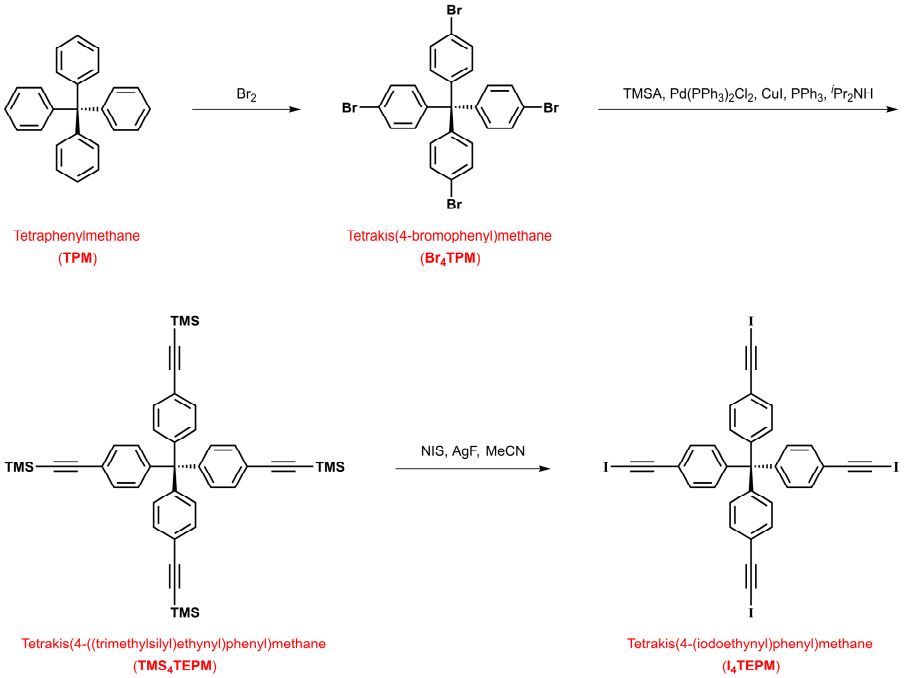

Scheme 3. Synthetic route to **TMS$_4$TEPM** and **I$_4$TEPM**.

Both **I$_4$TEPM** and **I$_4$TEPA** were accessible from the corresponding TMS derivatives, **TMS$_4$TEPM** and **TMS$_4$TEPA**, via one-pot/in situ desilylative iodination using silver(I) fluoride and *N*-iodosuccinimide. This direct trimethylsilyl-to-iodo transformation allowed us to avoid potentially unstable ethynyl intermediates and to achieve the target compounds in moderate yields (56% and 63%, respectively). Even though the ^{1}H and proton-decoupled ^{13}C-NMR spectra of these four-fold symmetric tetraiodoethynyl species are quite simple, the signals display considerable solvent dependency due to

their XB-based complexation ability, with the alkynyl carbon bonded to iodine being most strongly affected (**I_4TEPM**: 7.0 ppm in $CDCl_3$ versus 18.4 ppm in DMSO-d_6, **I_4TEPA**: 6.2 ppm in $CDCl_3$ versus 17.0 ppm in DMSO-d_6). It is also worth mentioning that the ^{1}H-NMR spectrum of **I_4TEPA** exhibits conspicuous second order (leaning/roofing) effects.

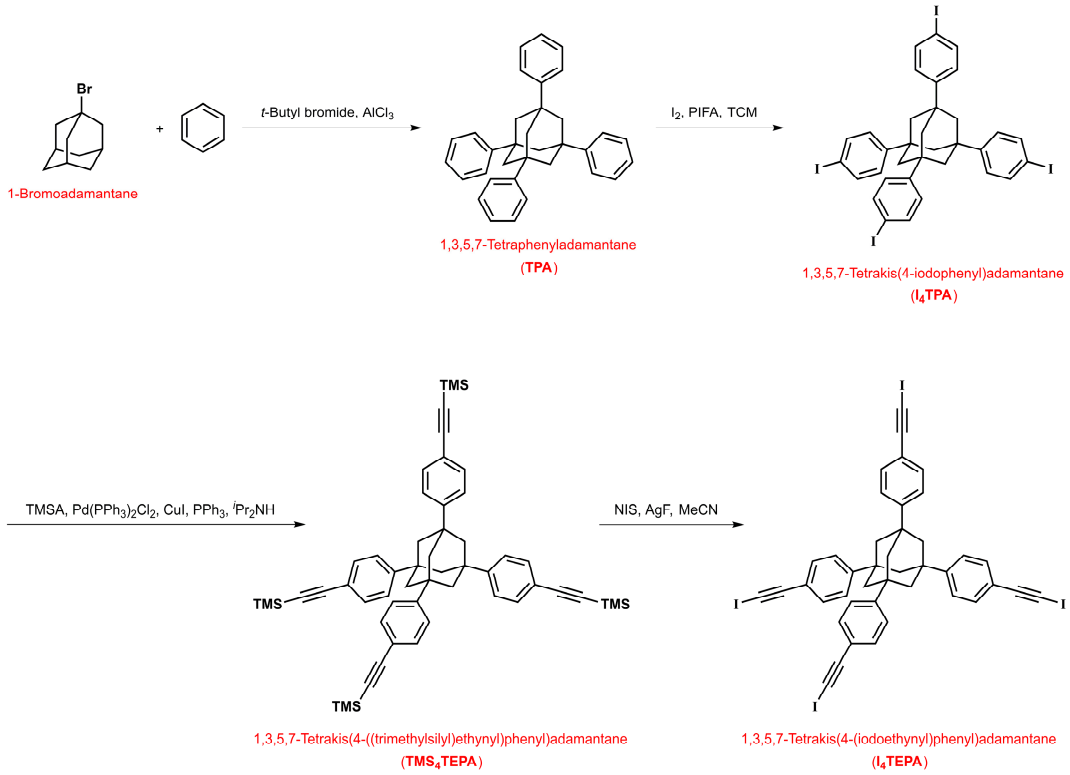

Scheme 4. Synthetic route to **TMS_4TEPA** and **I_4TEPA**.

Crystals of **TMS_4TEPM** suitable for single-crystal X-ray analysis were obtained by slow evaporation of either tetrahydrofuran/ethanol or chloroform/ethanol solution. For **TMS_4TEPA**, X-ray quality crystals could be harvested from hexane, heptane, heptane/dichloromethane or chloroform/ethanol. As anticipated, structural determination revealed that both are somewhat porous in nature (14.9% and 14.5% free volume, respectively). They, however, do not form empty-channel structures; instead, they have disconnected spatial voids or "porosity without pores", as described by Barbour (Figure 1) [53]. The overall packing is mainly mediated by extensive phenyl embraces.

In order to get some insight about the electron density/charge distribution over the free tetraiodoethynyl tectons and the degree of activation of XB donor sites (i.e., iodine atoms) delivered by *sp*-hybridized carbons [35–38], their molecular electrostatic potential (MEP) maps were generated (Figure 2). As expected, both **I_4TEPM** and **I_4TEPA** were found to have well-built σ-holes (+172.4 and +170.7 kJ/mol, respectively) on each iodine atom. Indeed, these σ-hole potential values are significantly higher than those of other closely-related tetra-halogenated molecules (see Supplementary Materials, Figure S33).

We then tried to grow crystals of **I_4TEPM** and **I_4TEPA** but were successful only with the former. The structural analysis of **I_4TEPM** crystals (harvested from hexanes) showed that the molecules are arranged in stacks which, in turn, are linked together by C≡C–I···(C≡C) halogen bonds, with near orthogonal approach of C–I donors towards C≡C triple bonds (detailed geometrical data are given in Table 1). In each **I_4TEPM** molecule, only two iodoethynyl arms participate in these T-shaped contacts, and the remaining two form weak C≡C–I···π(phenyl) interactions. The extended (and possibly cooperative) *zigzag* arrays of the C≡C–I···π(ethynyl) interactions ultimately make ladder-like motifs between individual molecular rows, leading to an infinite two-dimensional network (Figure 3 left).

I_4TEPM shares these packing features with its bromo analog, tetrakis(4-(bromoethynyl)phenyl)methane (**Br_4TEPM**) [42], but not with tetrakis(4-ethynylphenyl)methane (**TEPM**), which forms an interwoven diamondoid net [44].

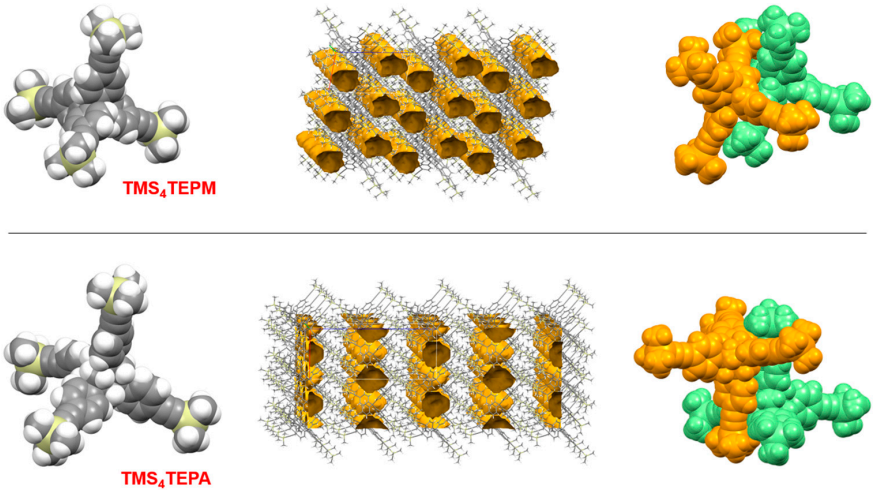

Figure 1. Crystal structures of **TMS_4TEPM** and **TMS_4TEPA**. (from left) Single molecules, overall packing and phenyl embraces (representative structures are shown from disordered structures).

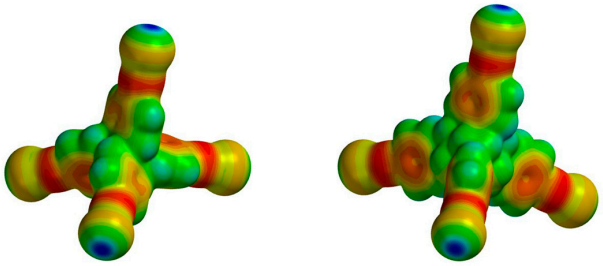

Figure 2. Molecular electrostatic potential (MEP) surfaces of the free tetraiodoethynyl tectons, **I_4TEPM** and **I_4TEPA**. Both plots have been set to the same color scale for visual comparison. Range: from −80 kJ/mol (red) to +175 kJ/mol (blue).

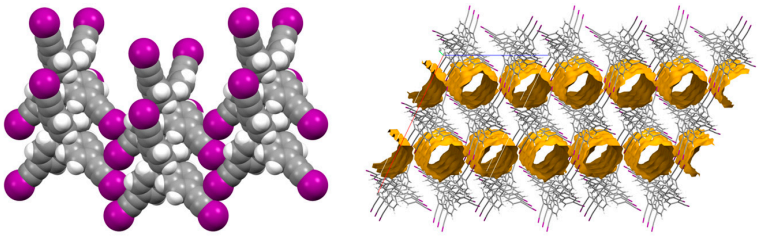

Figure 3. Crystal structure of **I_4TEPM**, showing halogen bonding (XB)-driven network formation (left) and void space in overall packing (right).

In contrast to the structure of **TMS_4TEPM** with isolated voids, **I_4TEPM** possesses one-dimensional channels along the crystallographic *b* axis (Figure 3 right). These channels account for 26.5% of the crystal volume, which is roughly twice as high as that of **TMS_4TEPM**. Another point worth emphasizing is that the precursor molecules, tetraphenylmethane (**TPM**), tetrakis(4-bromophenyl)methane (**Br_4TPM**) and tetrakis(4-iodophenyl)methane (**I_4TPM**), all form non-porous structures (see Supplementary Materials, Figure S34), highlighting the effectiveness of our strategy.

Since MPMs are usually held together by relatively weak interactions, they are not as rigid and robust as zeolites, metal-organic frameworks (MOFs) or covalent-organic frameworks (COFs). In most cases, attempts at activation (i.e., removal of entrapped guest molecules) cause structural disintegration. Hence, the real challenge lies in attaining permanently porous molecular materials that can behave analogously to framework-type solids. Most importantly, **I_4TEPM**, sustained primarily by the iodoethynyl catemer motif (i.e., the infinite C≡C–I···C≡C–I··· synthon), can maintain its structural integrity upon guest solvent loss, indicating its potential to exhibit permanent porosity.

In addition to tectonic construction, we also wanted to test the suitability of **I_4TEPM** in modular construction by co-crystallizing it with appropriate Lewis basic (i.e., XB-accepting) co-formers, in order to realize multicomponent architectures. With tetraphenylphosphonium halide salts ($Ph_4P^+X^-$; X^- = Cl^-, Br^-, I^-), it readily afforded diamondoid (**dia**) frameworks, but interpenetration and the inclusion of bulky Ph_4P^+ cations gave rise to highly compact arrangements within those solids [54]. As a charge-neutral co-crystallizing partner, our first choice was pyridine, one of the simplest XB acceptors, even though it cannot lead **I_4TEPM** to a polymeric assembly. We managed to get a binary crystalline material (confirmed by IR, NMR and TGA) but the structural characterization was not successful, as those crystals were quite fragile and rapidly deteriorated during data collection. This intrigued us to try out other Lewis basic/coordinating solvents with multiple bond forming ability. In three cases, with tetrahydrofuran (THF), dimethyl sulfoxide (DMSO) and 1,4-dioxane, **I_4TEPM** afforded crystalline binary solids.

Crystallization of **I_4TEPM** in THF/methanol afforded crystals of **I_4TEPM**·2THF where each THF molecule forms two halogen bonds in a bifurcated manner and connect adjacent **I_4TEPM** molecules together, thereby forming a one-dimensional twisted ribbon-like architecture (Figure 4a left). The resulting lattice comprises isolated voids that account for 14.4% of unit cell volume (Figure 4a right).

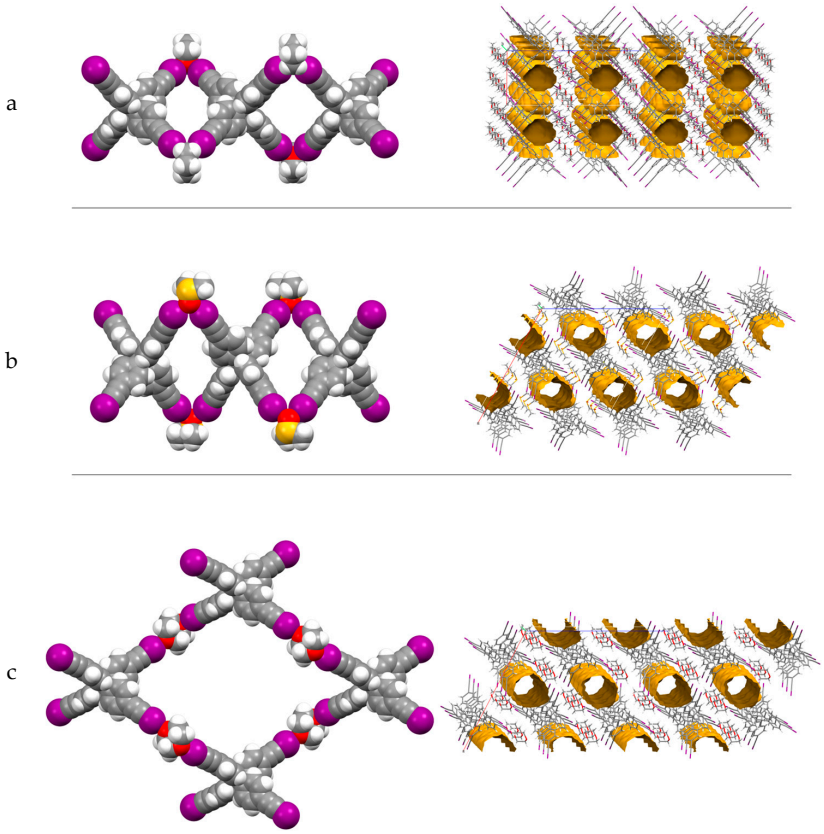

Figure 4. Crystal structures of (**a**) **I_4TEPM**·2THF, (**b**) **I_4TEPM**·2DMSO and (**c**) **I_4TEPM**·2Dioxane, showing XB-directed chain/net formation (left) and void space in overall packing (right).

Crystallization of **I$_4$TEPM** from neat DMSO or DMSO/methanol yielded crystals of **I$_4$TEPM**·2DMSO which has XB interactions analogous to those observed in **I$_4$TEPM**·2THF. Once again, the coordinating solvent acts as a bridging ligand and gives rise to a twisted-ribbon supramolecular chain (Figure 4b left), with one-dimensional channels of 21.0% free volume in the overall packing (Figure 4b right).

By using 1,4-dioxane/dichloromethane as the solvent system, crystals of **I$_4$TEPM**·2Dioxane could be obtained. As expected, dioxane serves as a linear ditopic ligand, so the structure propagates into two dimensions (Figure 4c left). As in **I$_4$TEPM**·2DMSO, the structure creates one-dimensional channels parallel to the crystallographic *c* axis, holding 21.0% free volume (Figure 4c right).

Unfortunately, as is the case with many other crystalline solvates, all these binary crystals are unstable at room temperature. Once removed from the mother liquor, they gradually become opaque because of the partial loss of halogen-bonded and freely-occupying solvent molecules. The DSC and TGA thermograms (Figure 5), however, show that the solvents are somewhat strongly attached to the crystal lattice. In particular, for **I$_4$TEPM**·2THF and **I$_4$TEPM**·2Dioxane, the removal temperatures are noticeably higher than their respective boiling points.

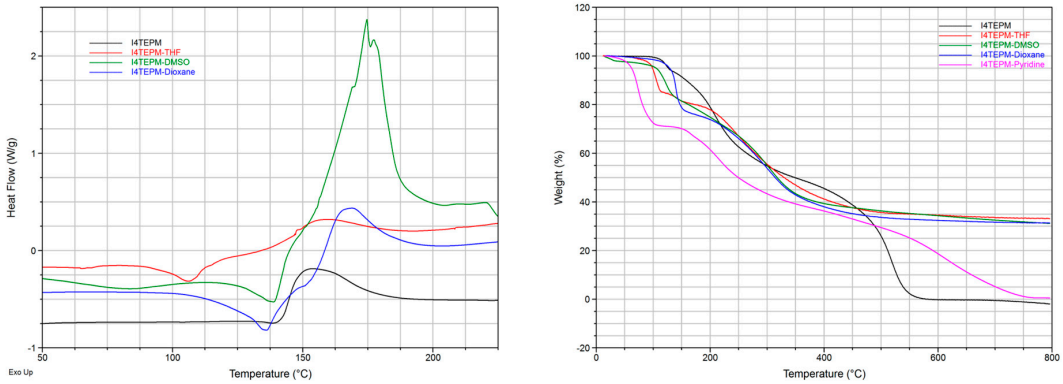

Figure 5. (**left**) DSC traces (Tzero aluminum pan, 1–2 mg sample size, 5 °C·min^{-1} heating rate, nitrogen atmosphere) and (**right**) TGA traces (platinum pan, 5–10 mg sample size, 10 °C·min^{-1} heating rate, nitrogen atmosphere).

Table 1 presents XB distances and angles of **I$_4$TEPM** and its binary crystals/solvates, along with the normalized distance (*ND*) and the percent radii reduction (%*RR*) values, which are two common indicators used as rough measures of the XB strength. In **I$_4$TEPM**, C≡C–I···(C≡C) interactions are not symmetric and the C–I donors reach more toward terminal acetylenic carbons. Consequently, one I···C separation is significantly longer (with a low %*RR* value) and deviates from linearity. The %*RR* values calculated for XBs observed in the three solvates are greater than 15% (except in one case), reflecting the moderate strength of those interactions. Moreover, all bonds have near-linear (> 170° angles, again one exception) arrangements, reflecting their high directionality.

Table 1. XB interaction parameters in the studied crystal structures.

Compound	C–I···O	*d*(I···O)/Å	*ND* [a]	*%RR* [b]	∠(C–I···O)/°
I$_4$TEPM	C9–I10···C8(π) [c]	3.405(12)	0.925	7.47	165.5(4)
	C9–I10···C9(π) [c]	3.266(13)	0.888	11.2	173.6(5)
I$_4$TEPM·2THF	C9–I10···O11 [d]	2.965(5)	0.847	15.3	170.1(3)
I$_4$TEPM·2DMSO	C9–I10···O23 [e]	3.013(3)	0.861	13.9	162.0(14)
	C18–I19···O23 [f]	2.797(3)	0.799	20.1	170.0(14)
I$_4$TEPM·2Dioxane	C1–I1···O1	2.773(4)	0.792	20.8	174.3(11)
	C17–I2···O2 [g]	2.819(3)	0.805	19.5	174.4(9)

[a] Normalized distance, $ND = d_{xy}/(r_x + r_y)$, where d_{xy} is the crystallographically determined XB distance, and r_x and r_y are the van der Waals radii for the two involved atoms (I = 1.98 Å, C = 1.70 Å, O = 1.52 Å). [b] Percent radii reduction, $\%RR = (1 - ND) \times 100$. Symmetry transformations used to generate equivalent atoms: [c] 1−x, $\frac{1}{2}$+y, 1.5−z. [d] $\frac{1}{2}$+x, 1.5−y, 1−z. [e] $-\frac{1}{2}$+x, $-\frac{1}{2}$−y, $-\frac{1}{2}$+z. [f] x, 1+y, z. [g] $-\frac{1}{2}$+x, −2.5+y, $-\frac{1}{2}$+z.

3. Conclusions

The solid-state packing behavior of tetrakis(4-((trimethylsilyl)ethynyl)phenyl)methane [**TMS$_4$TEPM**] and 1,3,5,7-tetrakis(4-((trimethylsilyl)ethynyl)phenyl)adamantane [**TMS$_4$TEPA**] showed some degree of extrinsic porosity. These two molecules were converted into tecton-like derivatives with XB capability, **I$_4$TEPM** and **I$_4$TEPA**, in order to investigate the power of iodoethynyl recognition sites in the context of solid-state packing and extrinsic porosity. Our results demonstrate that, even though **I$_4$TEPA** tends not to form crystalline unary or binary solids, **I$_4$TEPM** crystallizes into porous solids in its neat form as well as with suitable co-formers. The binary systems formed with coordinating solvents (i.e., **I$_4$TEPM**·4Pyridine, **I$_4$TEPM**·2THF, **I$_4$TEPM**·2DMSO and **I$_4$TEPM**·2Dioxane) are prone to collapse upon solvent removal. It is therefore rational to think that **I$_4$TEPM** would offer more stable crystals if the co-formers employed are solids at ambient conditions. Efforts to explore these new possibilities, especially utilizing molecules with tetrahedrally-disposed XB accepting sites (e.g., tetraazaadamantane, tetrakis(4-pyridyl)cyclobutane, tetrakis(4-pyridyloxymethyl)methane) are currently being undertaken in our lab.

4. Materials and Methods

Unless otherwise noted, all reagents, solvents and precursors (tetraphenylmethane and 1-bromoadamantane) were purchased from commercial sources and used as received, without further purification. Nuclear magnetic resonance (NMR) spectra were recorded at room temperature on a Varian Unity Plus (400 MHz) spectrometer (Agilent Technologies, Inc., Santa Clara, CA, USA). Chemical shifts for ^{1}H-NMR spectra were referenced to the residual protio impurity peaks in the deuterated solvents, while ^{13}C{^{1}H} NMR spectra were referenced against the solvent ^{13}C resonances. A Nicolet 380 FT-IR system (Thermo Fisher Scientific Inc., Waltham, MA, USA) was used for the infrared (IR) spectroscopic analysis. Differential scanning calorimetry (DSC) and thermogravimetric analysis (TGA) were performed on TA Q20 and TA Q50 (TA Instruments, New Castle, DE, USA), respectively. In order to calculate the molecular surface electrostatic potentials of tetra-halogenated TPM and TPA species, their geometries were optimized (using Spartan '14 software [55]) at hybrid functional B3LYP/6-311+G** and B3LYP/6-311++G** levels of theory, respectively, and potential values were subsequently mapped onto 0.002 au isosurface. Detailed crystallographic information about data collections, solutions, and refinements can be found in the Supplementary Materials. Structural visualizations and void mapping were done using Mercury software [56]. For free volume calculations, the voids function in Mercury (with contact surface, 1.2 Å probe radius and 0.2 Å approximate grid spacing) and/or the solvent-masking tool in Olex2 (with its default parameters) were employed [56,57].

*4.1. Synthesis of Tetrakis(4-bromophenyl)methane (**Br_4TPM**)*

The bromination of tetraphenylmethane was performed neat using an excess of molecular bromine. To a 100-mL round-bottom flask containing tetraphenylmethane (2.00 g, 6.24 mmol, 1 equiv.), bromine liquid (6.4 mL, 124.8 mmol, 20 equiv.) was added carefully at 0 °C. After attaching a water-cooled reflux condenser, the resultant dark reddish slurry was stirred vigorously at room temperature for one hour, and then cooled to −78 °C by using a dry ice/acetone bath. Ethanol (25 mL) was added slowly and the reaction mixture was allowed to warm to room temperature overnight. Then, to destroy excess/unreacted bromine, it was treated with 40% aqueous solution of sodium bisulfite (approximately 75 mL) and stirred for an additional 30 min until the orange color disappeared. The tan colored solid was collected by filtration, washed well with distilled water (100 mL) and oven-dried at 60 °C for five hours. This solid was further purified by re-crystallization from chloroform/ethanol (2:1), affording tetrakis(4-bromophenyl)methane, **Br_4TPM,** as an off-white crystalline material. Yield: 3.65 g (5.74 mmol, 92%). ^{1}H-NMR (400 MHz, $CDCl_3$) δ (ppm): 7.39 (d, 8H); 7.01 (d, 8H). ^{13}C-NMR (100 MHz, $CDCl_3$) δ (ppm): 144.64, 132.57, 131.30, 121.02, 63.84. ATR-FTIR (cm^{-1}): 3059, 1919, 1569, 1478, 1395, 1185, 1077, 1007, 948, 808, 753.

*4.2. Synthesis of Tetrakis(4-((trimethylsilyl)ethynyl)phenyl)methane (**TMS_4TEPM**)*

This step involved a Sonogashira cross-coupling reaction of tetrakis(4-bromophenyl)methane with trimethylsilylacetylene. Tetrakis(4-bromophenyl)methane (3.50 g, 5.50 mmol, 1 equiv.) and triphenylphosphine (462 mg, 1.76 mmol, 32 mol%) were placed in a 250-mL round-bottomed flask. Diisopropyl amine (100 mL) was added and the resulting solution was purged with dinitrogen gas for 30 min. Then, bis(triphenylphosphine)palladium(II) dichloride (618 mg, 0.88 mmol, 16 mol%), copper(I) iodide (168 mg, 0.88 mmol, 16 mol%) and trimethylsilylacetylene (6.2 mL, 44.0 mmol, 8 equiv.) were added. The reaction flask was fitted to a water-jacketed condenser, cooled to −78 °C, subjected to a brief vacuum/backfill cycle and refluxed for 24 h under nitrogen atmosphere. After removing volatile materials in vacuo, the residue was re-dissolved in chloroform (100 mL) and filtered through a pad of Celite, using an extra 50 mL portion of chloroform to wash the filter pad. The combined filtrate was then washed with distilled water (2 × 25 mL) and brine (25 mL), dried over anhydrous magnesium sulfate, and evaporated to dryness under vacuum. The crude product was flash-column-chromatographed on silica gel using pure hexanes followed by hexanes/ethyl acetate (4:1) as eluents to obtain the title compound, **TMS_4TEPM,** as a pale yellowish solid. Yield: 3.30 g (4.68 mmol, 85%). ^{1}H-NMR (400 MHz, $CDCl_3$) δ (ppm): 7.33 (d, 8H), 7.05 (d, 8H), 0.24 (s, 36H). ^{13}C-NMR (100 MHz, $CDCl_3$) δ (ppm): 146.21, 131.59, 130.95, 121.42, 104.82, 95.00, 64.98, 0.18. ATR-FTIR (cm^{-1}): 2957, 2157, 1496, 1405, 1247, 1187, 1019, 835, 758.

*4.3. Synthesis of Tetrakis(4-(iodoethynyl)phenyl)methane (**I_4TEPM**)*

The one-pot/in situ desilylative iodination (i.e., direct trimethylsilyl-to-iodo conversion) method was employed. Acetonitrile (150 mL) was transferred into a 250-mL round-bottom flask that contained tetrakis(4-((trimethylsilyl)ethynyl)phenyl)methane (2.50 g, 3.54 mmol, 1 equiv.). The flask was wrapped in aluminium foil, and then silver(I) fluoride (2.70 g, 21.3 mmol, 6 equiv.) and *N*-iodosuccinimide (4.78 g, 21.3 mmol, 6 equiv.) were added. It was then evacuated (while stirring), refilled with nitrogen and stirred at room temperature for 24 h. Distilled water (200 mL) was added and the resulting mixture was extracted with diethyl ether (4 × 50 mL). The combined organic layers were washed with saturated sodium bisulfite (40 mL), distilled water (40 mL) and brine (40 mL), and dried over anhydrous magnesium sulfate. The evaporation of the solvent under reduced pressure resulted in an orange colored residue. Additional cleanup by column chromatography (silica gel, hexanes/ethyl acetate = 9:1) gave the desired compound, **I_4TEPM**, as a yellow solid. Crystals suitable for single-crystal X-ray diffraction were grown from hexanes. Yield: 1.83 g (1.98 mmol, 56%). ^{1}H-NMR (400 MHz, $CDCl_3$) δ (ppm): 7.32 (d, 8H), 7.06 (d, 8H). ^{13}C-NMR (100 MHz, $CDCl_3$) δ (ppm): 146.34, 132.04, 130.87,

121.81, 93.87, 65.02, 7.03. ^{1}H-NMR (400 MHz, DMSO-d_6) δ (ppm): 7.37 (d, 8H), 7.04 (d, 8H). ^{13}C-NMR (100 MHz, DMSO-d_6) δ (ppm): 145.68, 131.66, 130.36, 121.08, 92.11, 64.26, 18.41. ATR-FTIR (cm^{-1}): 2944, 2167, 1490, 1400, 1186, 1112, 1016, 955, 898, 827, 722.

*4.4. Synthesis of 1,3,5,7-Tetraphenyladamantane (**TPA**)*

In a 250-mL round-bottom flask, *tert*-butyl bromide (3.9 mL, 34.9 mmol, 2.5 equiv.) was added to a solution of 1-bromoadamantane (3.00 g, 13.9 mmol, 1 equiv.) in anhydrous benzene (30 mL). The flask was placed in an ice bath and aluminium chloride (186 mg, 1.39 mmol, 10 mol%) was carefully charged to the chilled stirring solution. The mixture was then heated under reflux until the evolution of hydrogen bromide ceased (the top of the condenser was connected to a gas absorption trap containing 30% aqueous sodium hydroxide). The resultant heterogeneous mixture was allowed to cool to room temperature and filtered, and the residue was washed sequentially with chloroform (30 mL), water (50 mL) and chloroform (30 mL). The off-white solid was further purified by washing overnight with refluxing chloroform in a Soxhlet apparatus, which gave 1,3,5,7-tetraphenyladamantane, **TPA**, as a fine white powder. Yield: 5.04 g (11.4 mmol, 82%). Mp: > 300 °C. ATR-FTIR (cm^{-1}): 3055, 3020, 2918, 2849, 1597, 1493, 1442, 1355, 1263, 1078, 1030, 918, 889, 844, 788, 760, 746, 699.

*4.5. Synthesis of 1,3,5,7-Tetrakis(4-iodophenyl)adamantane (**I$_4$TPA**)*

To a 250-mL round-bottom flask containing a suspension of 1,3,5,7-tetraphenyladamantane (4.00 g, 9.08 mmol, 1 equiv.) in chloroform (100 mL) was added iodine (5.76 g, 22.7 mmol, 2.5 equiv.). This mixture was stirred vigorously at room temperature until the iodine fully dissolved. The flask was flushed with nitrogen gas and bis(trifluoroacetoxy)iodo)benzene (9.76 g, 22.7 mmol, 2.5 equiv.) was added. The resulting mixture was stirred at room temperature for 12 h. It was then filtered off, and the collected solid was washed with an excess amount of chloroform (200 mL). The combined dark purple filtrate was washed with 5% sodium bisulfite solution twice (2 × 50 mL), followed by distilled water (100 mL) and saturated sodium chloride solution (100 mL). It was dried with anhydrous magnesium sulfate and the solvent was removed under reduced pressure, which resulted in a pale-yellow solid. After refluxing in methanol (200 mL) for 12 h, the pure compound, **I$_4$TPA**, was isolated as a white solid by filtration and air-drying. Yield: 5.91 g (6.26 mmol, 69%). ^{1}H-NMR (400 MHz, $CDCl_3$) δ (ppm): ^{1}H-NMR (400 MHz, $CDCl_3$) δ (ppm): 7.67 (d, 8H), 7.18 (d, 8H), 2.06 (s, 12H). ^{13}C-NMR (100 MHz, $CDCl_3$) δ (ppm): 148.63, 137.75, 127.34, 91.96, 46.92, 39.29. ATR-FTIR (cm^{-1}): 3046, 2928, 2898, 2851, 1900, 1782, 1647, 1579, 1483, 1441, 1390, 1355, 1180, 1120, 1064, 1001, 888, 819, 775, 701, 659.

*4.6. Synthesis of 1,3,5,7-Tetrakis(4-((trimethylsilyl)ethynyl)phenyl)adamantane (**TMS$_4$TEPA**)*

As in the synthesis of **TMS$_4$TEPM**, this step involved a four-fold Sonogashira cross-coupling reaction of 1,3,5,7-tetrakis(4-iodophenyl)adamantane (**I$_4$TPA**) with trimethylsilylacetylene. Yield: 88%. ^{1}H-NMR (400 MHz, $CDCl_3$) δ (ppm): ^{1}H-NMR (400 MHz, $CDCl_3$) δ (ppm): 7.45 (d, 8H), 7.38 (d, 8H), 2.09 (s, 12H), 0.24 (s, 36H). ^{13}C-NMR (100 MHz, $CDCl_3$) δ (ppm): 149.63, 132.29, 125.13, 121.32, 105.19, 94.20, 46.97, 39.53, 0.25. ATR-FTIR (cm^{-1}): 3033, 2958, 2897, 2852, 2155, 1604, 1502, 1445, 1398, 1355, 1248, 1115, 1016, 859, 835, 758.

*4.7. Synthesis of 1,3,5,7-Tetrakis(4-(iodoethynyl)phenyl)adamantane (**I$_4$TEPA**)*

The same one-pot desilylative iodination method described above for the synthesis of **I$_4$TEPM** (i.e., the direct trimethylsilyl-to-iodo transformation using silver(I) fluoride and *N*-iodosuccinimide) was employed. Yield: 63%. ^{1}H-NMR (400 MHz, $CDCl_3$) δ (ppm): 7.42 (d, 8H), 7.39 (d, 8H), 2.09 (s, 12H). ^{13}C-NMR (100 MHz, $CDCl_3$) δ (ppm): 149.82, 132.64, 125.16, 121.57, 94.16, 46.88, 39.50, 6.18. ^{1}H-NMR (400 MHz, DMSO-d_6) δ (ppm): 7.51 (d, 8H), 7.37 (d, 8H), 2.00 (s, 12H). ^{13}C-NMR (100 MHz, DMSO-d_6) δ (ppm): 150.14, 131.74, 125.48, 120.50, 92.59, 45.48, 38.95, 17.02. ATR-FTIR (cm^{-1}): 3033, 2919, 2896, 2849, 2165, 1908, 1701, 1603, 1501, 1439, 1355, 1241, 1176, 1115, 1016, 837, 822, 769, 693.

*4.8. Synthesis of **I$_4$TEPM**·4pyridine*

In a 2-dram glass vial, **I$_4$TEPM** (10 mg, 0.011 mmol) was dissolved in 0.5 mL of pyridine. This open vial was placed in a second larger container (50-mL glass jar) containing 10 mL of pyridine/methanol (1:4) mixture. The outer container was then closed/sealed, and the apparatus was kept at ambient conditions to allow the vapor from methanol (anti-solvent) to diffuse into the sample solution. When the total volume of the inner vial became ~3 mL, it was taken out and, after partially tightening the lid, left undisturbed at ambient conditions to allow the solvents to evaporate slowly. Colorless/pale-yellow crystals were observed after few days. ATR-FTIR (cm^{-1}): 3032, 2923, 2851, 2158, 1909, 1587, 1493, 1438, 1405, 1210, 1185, 1147, 1066, 1017, 997, 955, 827, 745, 699.

*4.9. Synthesis of **I$_4$TEPM**·2THF*

In a 2-dram glass vial, **I$_4$TEPM** (10 mg, 0.011 mmol) was dissolved in 1 mL of tetrahydrofuran. After adding 1 mL of methanol, the vial (with a partially-tightened screw cap) was left undisturbed at ambient conditions to allow the solvents to evaporate slowly. Colorless/pale-yellow crystals suitable for single-crystal X-ray diffraction were observed after few days. ATR-FTIR (cm^{-1}): 2974, 2865, 2165, 1684, 1588, 1494, 1423, 1404, 1365, 1190, 1115, 1044, 1018, 884, 830, 809.

*4.10. Synthesis of **I$_4$TEPM**·2DMSO*

In a 2-dram glass vial, **I$_4$TEPM** (10 mg, 0.011 mmol) was dissolved in 0.5 mL of dimethyl sulfoxide. The vial (with a partially-tightened screw cap) was then allowed to stand at room temperature for one week, during which time colorless/pale-yellow crystals suitable for single-crystal X-ray diffraction were appeared. ATR-FTIR (cm^{-1}): 3032, 2986, 2908, 2160, 1494, 1429, 1398, 1308, 1186, 1113, 1039, 1014, 945, 826, 697.

*4.11. Synthesis of **I$_4$TEPM**·2dioxane*

In a 2-dram glass vial, **I$_4$TEPM** (10 mg, 0.011 mmol) was suspended in 0.5 mL 1,4-dioxane. After adding a few drops of methylene chloride, the vial was sealed and heated to obtain a clear solution. Colorless/pale-yellow crystals suitable for single-crystal X-ray diffraction were harvested by slow evaporation. ATR-FTIR (cm^{-1}): 2958, 2906, 2851, 2171, 1490, 1448, 1401, 1369, 1288, 1252, 1186, 1113, 1077, 1016, 976, 866, 829, 735.

Supplementary Materials: NMR and IR spectra, and crystallographic data are available online at http://www.mdpi.com/2624-8549/2/1/11/s1. The crystallographic data for this paper (CCDC 1971906–1971911) can also be obtained free of charge via www.ccdc.cam.ac.uk/data_request/cif, or by emailing data_request@ccdc.cam.ac.uk, or by contacting The Cambridge Crystallographic Data Centre, 12 Union Road, Cambridge CB2 1EZ, UK; fax: +44 1223 336033.

Author Contributions: C.A.G. and C.B.A. conceived and designed the experiments; C.A.G. performed the experiments; A.S.S. and E.W.R. performed the single-crystal X-ray crystallography; C.A.G. and C.B.A. analyzed the data and wrote the paper. All authors have read and agreed to the published version of the manuscript.

Funding: This research was funded by the U. S. Army Research Laboratory and the U. S. Army Research Office, grant number W911NF-13-1-0387.

Acknowledgments: We are grateful to Victor W. Day at the University of Kansas for collecting some single-crystal X-ray data. He, in turn, acknowledges the NSF-MRI grant CHE-0923449 which was used to purchase an X-ray diffractometer and software used in this study.

Conflicts of Interest: The authors declare no conflict of interest. The funders had no role in the design of the study; in the collection, analyses, or interpretation of data; in the writing of the manuscript, or in the decision to publish the results.

References

1. Kitaigorodskii, A.I. *Molecular Crystals and Molecules*; Academic Press: New York, NY, USA, 1973.
2. Kitaigorodskii, A.I. *Organic Chemical Crystallography*; Consultants Bureau: New York, NY, USA, 1961.

3. Kitaigorodskii, A.I. Non-bonded interactions of atoms in organic crystals and molecules. *Chem. Soc. Rev.* **1978**, *7*, 133–163. [CrossRef]
4. Kitaigorodskii, A.I. The principle of close packing and the condition of thermodynamic stability of organic crystals. *Acta Crystallogr.* **1965**, *18*, 585–590. [CrossRef]
5. Kitaigorodskii, A.I. The close-packing of molecules in crystals of organic compounds. *J. Phys. (USSR)* **1945**, *9*, 351–352.
6. Lü, J.; Cao, R. Porous organic molecular frameworks with extrinsic porosity: A platform for carbon storage and separation. *Angew. Chem. Int. Ed.* **2016**, *55*, 9474–9480. [CrossRef] [PubMed]
7. Hashim, M.I.; Hsu, C.-W.; Le, H.T.M.; Miljanić, O.Š. Organic molecules with porous crystal structures. *Synlett* **2016**, *27*, 1907–1918.
8. Tian, J.; Thallapally, P.K.; McGrail, B.P. Porous organic molecular materials. *CrystEngComm* **2012**, *14*, 1909–1919. [CrossRef]
9. Mastalerz, M. Permanent porous materials from discrete organic molecules—towards ultra-high surface areas. *Chem. Eur. J.* **2012**, *18*, 10082–10091. [CrossRef]
10. McKeown, N.B. Nanoporous molecular crystals. *J. Mater. Chem.* **2010**, *20*, 10588–10597. [CrossRef]
11. Holst, J.R.; Trewin, A.; Cooper, A.I. Porous organic molecules. *Nat. Chem.* **2010**, *2*, 915–920. [CrossRef]
12. Hasell, T.; Cooper, A.I. Porous organic cages: Soluble, modular and molecular pores. *Nat. Rev. Mater.* **2016**, *1*, 16053. [CrossRef]
13. Evans, J.D.; Sumby, C.J.; Doonan, C.J. Synthesis and applications of porous organic cages. *Chem. Lett.* **2015**, *44*, 582–588. [CrossRef]
14. Zhang, G.; Mastalerz, M. Organic cage compounds—from shape-persistency to function. *Chem. Soc. Rev.* **2014**, *43*, 1934–1947. [CrossRef] [PubMed]
15. Imashiro, F.; Yoshimura, M.; Fujiwara, T. 'Guest-free' Dianin's compound. *Acta Crystallogr. C* **1998**, *54*, 1357–1360. [CrossRef]
16. Barrer, R.M.; Shanson, V.H. Dianin's compound as a zeolitic sorbent. *J. Chem. Soc. Chem. Commun.* **1976**, 333–334. [CrossRef]
17. Kaleta, J.; Bastien, G.; Wen, J.; Dračínský, M.; Tortorici, E.; Císařová, I.; Beale, P.D.; Rogers, C.T.; Michl, J. Bulk inclusions of double pyridazine molecular rotors in hexagonal tris(*o*-phenylene)cyclotriphosphazene. *J. Org. Chem.* **2019**, *84*, 8449–8467. [CrossRef]
18. Sozzani, P.; Bracco, S.; Comotti, A.; Ferretti, L.; Simonutti, R. Methane and carbon dioxide storage in a porous van der Waals crystal. *Angew. Chem. Int. Ed.* **2005**, *44*, 1816–1820. [CrossRef]
19. Allcock, H.R.; Siegel, L.A. Phosphonitrilic compounds. III. Molecular inclusion compounds of tris(*o*-phenylenedioxy)phosphonitrile trimer. *J. Am. Chem. Soc.* **1964**, *86*, 5140–5144. [CrossRef]
20. Msayib, K.J.; Book, D.; Budd, P.M.; Chaukura, N.; Harris, K.D.M.; Helliwell, M.; Tedds, S.; Walton, A.; Warren, J.E.; Xu, M.C.; et al. Nitrogen and hydrogen adsorption by an organic microporous crystal. *Angew. Chem. Int. Ed.* **2009**, *48*, 3273–3277. [CrossRef]
21. Wuest, J.D. Engineering crystals by the strategy of molecular tectonics. *Chem. Commun.* **2005**, 5830–5837. [CrossRef]
22. Hosseini, M.W. Molecular tectonics: From simple tectons to complex molecular networks. *Acc. Chem. Res.* **2005**, *38*, 313–323. [CrossRef]
23. Hosseini, M.W. Reflexion on molecular tectonics. *CrystEngComm* **2004**, *6*, 318–322. [CrossRef]
24. Su, D.; Wang, X.; Simard, M.; Wuest, J.D. Molecular tectonics. *Supramol. Chem.* **1995**, *6*, 171–178. [CrossRef]
25. Lin, R.-B.; He, Y.; Li, P.; Wang, H.; Zhou, W.; Chen, B. Multifunctional porous hydrogen-bonded organic framework materials. *Chem. Soc. Rev.* **2019**, *48*, 1362–1389. [CrossRef] [PubMed]
26. Hisaki, I.; Xin, C.; Takahashi, K.; Nakamura, T. Designing hydrogen-bonded organic frameworks (HOFs) with permanent porosity. *Angew. Chem. Int. Ed.* **2019**, *58*, 11160–11170. [CrossRef] [PubMed]
27. Luo, J.; Wang, J.-W.; Zhang, J.-H.; Lai, S.; Zhong, D.-C. Hydrogen-bonded organic frameworks: Design, structures and potential applications. *CrystEngComm* **2018**, *20*, 5884–5898. [CrossRef]
28. Han, Y.-F.; Yuan, Y.-X.; Wang, H.-B. Porous hydrogen-bonded organic frameworks. *Molecules* **2017**, *22*, 266. [CrossRef]
29. Mastalerz, M.; Oppel, I.M. Rational construction of an extrinsic porous molecular crystal with an extraordinary high specific surface area. *Angew. Chem. Int. Ed.* **2012**, *51*, 5252–5255. [CrossRef]

30. Fournier, J.H.; Maris, T.; Wuest, J.D. Molecular tectonics. Porous hydrogen-bonded networks built from derivatives of 9,9′-spirobifluorene. *J. Org. Chem.* **2004**, *69*, 1762–1775. [CrossRef]
31. Demers, E.; Maris, T.; Wuest, J.D. Molecular tectonics. Porous hydrogen-bonded networks built from derivatives of 2,2′,7,7′-tetraphenyl-9,9′-spirobi[9 *H*-fluorene]. *Cryst. Growth Des.* **2005**, *5*, 1227–1235. [CrossRef]
32. Chen, T.H.; Popov, I.; Kaveevivitchai, W.; Chuang, Y.C.; Chen, Y.S.; Daugulis, O.; Jacobson, A.J.; Miljanic, O.S. Thermally robust and porous noncovalent organic framework with high affinity for fluorocarbons and CFCs. *Nat. Commun.* **2014**, *5*. [CrossRef]
33. Shankar, S.; Chovnik, O.; Shimon, L.J.W.; Lahav, M.; van der Boom, M.E. Directed molecular structure variations of three-dimensional halogen-bonded organic frameworks (XBOFs). *Cryst. Growth Des.* **2018**, *18*, 1967–1977. [CrossRef]
34. Nikolayenko, V.I.; Castell, D.C.; van Heerden, D.P.; Barbour, L.J. Guest-induced structural transformations in a porous halogen-bonded framework. *Angew. Chem. Int. Ed.* **2018**, *57*, 12086–12091. [CrossRef] [PubMed]
35. Nguyen, S.T.; Ellington, T.L.; Allen, K.E.; Gorden, J.D.; Rheingold, A.L.; Tschumper, G.S.; Hammer, N.I.; Watkins, D.L. Systematic experimental and computational studies of substitution and hybridization effects in solid-state halogen bonded assemblies. *Cryst. Growth Des.* **2018**, *18*, 3244–3254. [CrossRef]
36. González, L.; Gimeno, N.; Tejedor, R.M.; Polo, V.; Ros, M.B.; Uriel, S.; Serrano, J.L. Halogen-bonding complexes based on bis(iodoethynyl)benzene units: A new versatile route to supramolecular materials. *Chem. Mater.* **2013**, *25*, 4503–4510. [CrossRef]
37. Aakeröy, C.B.; Baldrighi, M.; Desper, J.; Metrangolo, P.; Resnati, G. Supramolecular hierarchy among halogen-bond donors. *Chem. Eur. J.* **2013**, *19*, 16240–16247. [CrossRef]
38. Sarwar, M.G.; Dragisic, B.; Salsberg, L.J.; Gouliaras, C.; Taylor, M.S. Thermodynamics of halogen bonding in solution: Substituent, structural, and solvent effects. *J. Am. Chem. Soc.* **2010**, *132*, 1646–1653. [CrossRef]
39. Baldrighi, M.; Bartesaghi, D.; Cavallo, G.; Chierotti, M.R.; Gobetto, R.; Metrangolo, P.; Pilati, T.; Resnati, G.; Terraneo, G. Polymorphs and co-crystals of haloprogin: An antifungal agent. *CrystEngComm.* **2014**, *16*, 5897–5904. [CrossRef]
40. Lemouchi, C.; Vogelsberg, C.S.; Zorina, L.; Simonov, S.; Batail, P.; Brown, S.; Garcia-Garibay, M.A. Ultra-fast rotors for molecular machines and functional materials via halogen bonding: Crystals of 1,4-bis(iodoethynyl)bicyclo[2.2.2]octane with distinct gigahertz rotation at two sites. *J. Am. Chem. Soc.* **2011**, *133*, 6371–6379. [CrossRef]
41. Dunitz, J.D.; Gehrer, H.; Britton, D. The crystal structure of diiodacetylene: An example of pseudosymmetry. *Acta Crystallogr. B* **1972**, *28*, 1989–1994. [CrossRef]
42. Guo, W.Z.; Galoppini, E.; Gilardi, R.; Rydja, G.I.; Chen, Y.H. Weak intermolecular interactions in the crystal structures of molecules with tetrahedral symmetry: Diamondoid nets and other motifs. *Cryst. Growth Des.* **2001**, *1*, 231–237. [CrossRef]
43. Kaleta, J.; Bastien, G.; Císařová, I.; Batail, P.; Michl, J. Molecular rods: Facile desymmetrization of 1,4-diethynylbicyclo[2.2.2]octane. *Eur. J. Org. Chem.* **2018**, *2018*, 5137–5142. [CrossRef]
44. Galoppini, E.; Gilardi, R. Weak hydrogen bonding between acetylenic groups: The formation of diamondoid nets in the crystal structure of tetrakis(4-ethynylphenyl)methane. *Chem. Commun.* **1999**, 173–174. [CrossRef]
45. Dikundwar, A.G.; Sathishkumar, R.; Guru Row, T.N.; Desiraju, G.R. Structural variability in the monofluoroethynylbenzenes mediated through interactions involving "organic" fluorine. *Cryst. Growth Des.* **2011**, *11*, 3954–3963. [CrossRef]
46. Thakur, T.S.; Sathishkumar, R.; Dikundwar, A.G.; Guru Row, T.N.; Desiraju, G.R. Third polymorph of phenylacetylene. *Cryst. Growth Des.* **2010**, *10*, 4246–4249. [CrossRef]
47. Dziubek, K.; Podsiadło, M.; Katrusiak, A. Nearly isostructural polymorphs of ethynylbenzene: Resolution of ≡CH···π(arene) and cooperative ≡CH···π(C≡C) interactions by pressure freezing. *J. Am. Chem. Soc.* **2007**, *129*, 12620–12621. [CrossRef] [PubMed]
48. Saha, B.K.; Nangia, A. Ethynyl group as a supramolecular halogen and C≡C–H···C≡C trimer synthon in 2,4,6-tris(4-ethynylphenoxy)-1,3,5-triazine. *Cryst. Growth Des.* **2007**, *7*, 393–401. [CrossRef]
49. Ohkita, M.; Suzuki, T.; Nakatani, K.; Tsuji, T. Polar assembly of 2,6-diethynylpyridine through C(sp^2)–H···N, C(sp)–H···π and π–π stacking interactions: Crystal structure and nonlinear optical properties. *Chem. Lett.* **2001**, *30*, 988–989. [CrossRef]

50. Robinson, J.M.; Kariuki, B.M.; Harris, K.D.; Philp, D. Interchangeability of halogen and ethynyl substituents in the solid state structures of di- and tri-substituted benzenes. *J. Chem. Soc. Perkin Trans.* **1998**, *2*, 2459–2470. [CrossRef]
51. Weiss, H.-C.; Bläser, D.; Boese, R.; Doughan, B.; Haley, M. C–H···π interactions in ethynylbenzenes: The crystal structures of ethynylbenzene and 1,3,5-triethynylbenzene, and a redetermination of the structure of 1,4-diethynylbenzene. *Chem. Commun.* **1997**, 1703–1704. [CrossRef]
52. Steiner, T.; Starikov, E.B.; Amado, A.M.; Teixeira-Dias, J.J.C. Weak hydrogen bonding. Part 2. The hydrogen bonding nature of short C–H···π contacts: Crystallographic, spectroscopic and quantum mechanical studies of some terminal alkynes. *J. Chem. Soc. Perkin Trans.* **1995**, *2*, 1321–1326. [CrossRef]
53. Barbour, L.J. Crystal porosity and the burden of proof. *Chem. Commun.* **2006**, *11*, 1163–1168. [CrossRef] [PubMed]
54. Gunawardana, C.A.; Đaković, M.; Aakeröy, C.B. Diamondoid architectures from halogen-bonded halides. *Chem. Commun.* **2018**, *54*, 607–610. [CrossRef] [PubMed]
55. Wavefunction, Inc. Irvine, CA 92612, USA. Available online: https://www.wavefun.com/spartan (accessed on 8 March 2020).
56. Macrae, C.F.; Sovago, I.; Cottrell, S.J.; Galek, P.T.A.; McCabe, P.; Pidcock, E.; Platings, M.; Shields, G.P.; Stevens, J.S.; Towler, M.; et al. Mercury 4.0: From visualization to analysis, design and prediction. *J. Appl. Crystallogr.* **2020**, *53*, 226–235. [CrossRef] [PubMed]
57. Dolomanov, O.V.; Bourhis, L.J.; Gildea, R.J.; Howard, J.A.K.; Puschmann, H. Olex2: A complete structure solution, refinement and analysis program. *J. Appl. Crystallogr.* **2009**, *42*, 339–341. [CrossRef]